Abnormal fetal muscle forces result in defects in spinal curvature and alterations in vertebral segmentation and shape

Short title: Fetal movements for spinal development

Rebecca A. Rolfe[1], James H. Bezer[1], Tyler Kim[1], Ahmed Z. Zaidon[1], Michelle L. Oyen[2], James C. Iatridis[3], Niamh C. Nowlan[1]

1. Department of Bioengineering, Imperial College London, London, United Kingdom
2. Engineering Department, University of Cambridge, Cambridge, United Kingdom
3. Department of Orthopaedics, Icahn School of Medicine at Mount Sinai, New York, NY 10029

Correspondence: Dr Niamh Nowlan
Phone: +44 (0) 20 759 45189
E-mail: n.nowlan@imperial.ac.uk

Author Contributions:

RR carried out experiments, analyzed the data, and drafted the manuscript. NN, JI and MO were involved in conception of the present study and contributed to discussions of the findings and drafting of the manuscript. TK and AZZ contributed to the experiments and JB contributed to the data analysis. NN participated in data analysis and oversaw drafting of the manuscript. All authors read and approved the final manuscript.

ABSTRACT

The incidence of congenital spine deformities, including congenital scoliosis, kyphosis and lordosis, may be influenced by the *in utero* mechanical environment, and particularly by fetal movements at critical time-points. There is a limited understanding of the influence of fetal movements on spinal development, despite the fact that mechanical forces have been shown to play an essential role in skeletal development of the limb. This study investigates the effects of muscle forces on spinal curvature, vertebral segmentation and vertebral shape by inducing rigid or flaccid paralysis in the embryonic chick. The critical time-points for the influence of fetal movements on spinal development were identified by varying the time of onset of paralysis. Prolonged rigid paralysis induced severe defects in the spine, including curvature abnormalities, posterior and anterior vertebral fusions and altered vertebral shape, while flaccid paralysis did not affect spinal curvature or vertebral segmentation. Early rigid paralysis resulted in more severe abnormalities in the spine than later rigid paralysis. The findings of this study support the hypothesis that the timing and nature of fetal muscle activity are critical influences on the normal development of the spine, with implications for the understanding of congenital spine deformities.

KEYWORDS

Development, congenital spine deformities, chick immobilization, rigid paralysis, flaccid paralysis, muscle forces

INTRODUCTION

A congenital spine deformity is an abnormality of the postnatal spine in which abnormal curvature and deformations of the vertebrae occur[1-3]. Congenital scoliosis is the most common congenital spine deformity[1], while congenital kyphosis and lordosis, although rare, can have much more severe consequences than scoliosis if left untreated[2,3]. The incidence of congenital scoliosis is 0.5−1 per 1000 live births[3,4] and is classified as failed formation or incorrect segmentation of vertebrae, leading to full or partial vertebral fusion and subsequent alterations in spinal curvature[2]. The aetiology of congenital spine deformities is poorly understood, but is believed to be multifactorial, involving both genetic and environmental factors[5]. A number of environmental stimuli have been shown to have an influence on the development of congenital spinal deformities (reviewed in Li et al[6]), such as maternal exposures during pregnancy to hypoxia[7], carbon monoxide[8], and vitamin deficiency[6]. Conditions in which fetal movements are absent or abnormal indicate that the development of the spine could also depend on a normal pattern of fetal movements. A complete absence of fetal movement occurs in the rare, neonatal-lethal syndrome fetal akinesia deformation sequence (FADS) (also known as Pena-Shokeir syndrome)[9,10]. A range of spinal abnormalities in FADS cases has been reported and include underdevelopment of vertebral bodies[11], failure of formation of the cervical vertebrae[12] and abnormalities in spinal curvature[11,13-17]. Undiagnosed or mild congenital spinal deformities may also play an important role in adolescent idiopathic scoliosis, since even relatively small changes in curvature can lead to progressive scoliosis with vertebral body wedging due to asymmetric muscular loading during adolescent growth[18].

Mechanical stimulation has been shown to play an essential role in multiple aspects of skeletal development (reviewed in Nowlan et al. [19]), with decreased fetal movement leading to abnormal ossification patterns, loss of tissue definition in joint regions and altered rudiment shape[20-23]. In the developing chick spine, fusion of vertebrae and alterations in spinal curvature

have been reported following prolonged rigid paralysis[24-27]. Effects of immobility on the spine have also been briefly mentioned in mammalian models of abnormal fetal movements, including fusion of cervical vertebrae[28] and loss of joints in the cervical and lumbar regions[20]. However, curvature effects and vertebral shape changes have never been described in detail for any model system of abnormal fetal movements, and much remains unknown about the effects of the type of muscle forces and the critical timing of fetal movement on the developing spine. This study uses the pharmacologically paralyzed chick embryo model to determine the nature of mechanical stimulation due to muscle activity required for normal spinal curvature and vertebral segmentation and shape. The embryonic chick model is commonly used for investigating the role of fetal movements in skeletal development due to the ease of exogenous manipulation of the developing embryo. In contrast to the human spine, which consists of 7 cervical, 12 thoracic, 5 lumbar vertebrae and the sacrum and coccyx[29], the chick spine consists of 14 cervical, 7 thoracic, 7 lumbar, 7 sacral and 7 caudal vertebrae (Figure 1A). An important difference between the avian and the mammalian spine is that no involution of the notochord takes place, and no nucleus pulposus is present in the avian intervertebral disc (IVD)[30].

The hypothesis that fetal movements influence the development of the spine is tested by comparing the effects of prolonged rigid paralysis (constant static muscle forces without any dynamic component) and flaccid paralysis (no static or dynamic muscle forces) to development with normal fetal movements. Furthermore, we tested the hypothesis that earlier paralysis induces more severe effects on spine development than later paralysis, and aim to establish the critical time-points for the influence of muscle forces on spine development.

METHODS

In ovo paralysis

Fertilised eggs (DeKalb white, MedEggs, Norfolk, UK), were incubated at 37.5°C in a humidified incubator for 9 days. Controls were treated with 100µl of PBS plus 100units/ml antibiotic (Pen. Strep, Sigma, UK). 0.5% Decamethonium bromide (DMB) was used for rigid paralysis, or 5mg/ml Pancuronium bromide (PB), both dissolved in PBS plus 100units/ml antibiotic (Pen. Strep) (all Sigma, UK) for flaccid paralysis. Paralyzed embryos were visually monitored for movement daily, and no independent spontaneous movements were detected during monitoring. DMB is a neuromuscular blocking agent that induces rigid paralysis, where contraction of all skeletal muscle fibres is sustained, while PB induces flaccid paralysis wherein both dynamic and static forces are removed[31]. Neuromuscular blocking agents lead to a reduction in muscle size and contractile properties[32], and therefore, the static forces that would be experienced in the case of rigid paralysis would be substantially less than those experienced during normal dynamic muscle contractions. Treatments were delivered once every 24 hours in 100µl volumes that were administered on to the vasculature of the developing embryo. All experiments were performed in accordance with European Legislation (Directive 2010/63/EU), under which no license is required when working with embryos younger than two thirds gestation. Two types of paralysis regimen were applied; prolonged paralysis (treatment every 24 hours from embryonic day (E)3, equivalent to day 3 of incubation, until harvest at E9), and timed paralysis (varying day of initiation of paralysis). Prolonged paralysis was performed for both rigid and flaccid treatments, while timed paralysis was performed for rigid paralysis only. In the timed paralysis study, rigid paralysis was initiated at E3, 4, 5, 6, 7 or 8, and continued on consecutive days until E9. Euthanasia and harvesting of each specimen was performed by cutting the vasculature surrounding the embryo and placing it in ice cold PBS, following which the spines were carefully dissected.

Skeletal preparation, 3D scanning and image processing

Whole spines were stained in 0.015% alcian Blue in 95% Ethanol for 6–8 hours, and cleared in 1% Potassium Hydroxide (KOH) for 4–6 hours. Specimens were scanned in 3D using Optical Projection Tomography (OPT)[33]. 3D surface representations were produced for each spine using ImageJ[34]. In order to visualise curvature changes, these 3D representations were rotated so that the vertebral bodies and spinous processes were visible, and a line traced along the centres of the vertebral bodies to obtain an outline trace of the sagittal plane curvature. Next, the 3D representations were rotated so that the anterior aspect of the vertebral bodies were foremost and the posterior and lateral portions out of view, and a line traced along the centres of the vertebral bodies to provide an outline trace of the curvature in the coronal plane. Both sets of outline traces were aligned at thoracic vertebra 1 (T1).

Quantitative analysis of curvature in the sagittal plane

The geometric curvature (GC), where GC=1/ radius of curvature[35], was calculated for each vertebral body in the sagittal plane. For identifying the centre of each vertebra from the 3D data, each vertebra was individually aligned to a sagittal view such that the vertebral body and spinous processes were parallel. Within this plane, the virtual section which represented the mid-sagittal section of the notochord (which, in the chick spine, goes through the centre of the vertebral body) was identified. From this section, the point at the centre and halfway along the length of the notochord was taken as the x and y co-ordinates for the centre of the vertebra in the mid-sagittal section. Therefore, the points representing the centre of each vertebra are not precisely aligned in a single plane, but rather lie on the mid-planes bisecting each vertebral body. A curve was fitted to the vertebral coordinates using a cubic smoothing spline function, which places a third order polynomial around each point to fit an accurate curve across the data-set (MathWorks®, R2015a). Geometric curvature is defined for an arbitrary position on the spine as the reciprocal to the radius R of the osculating circle in 3D at that position and

represents the amount by which the 3D vertebral body-line deviates from being straight. The geometric curvature was obtained as previously described[35]:

$$GC(p) = \frac{\left|\frac{d\boldsymbol{C}(p)}{dp} \times \frac{d^2\boldsymbol{C}(p)}{dp^2}\right|}{\left|\frac{d\boldsymbol{C}(p)}{dp}\right|^3} = \frac{1}{R(p)}$$

where ***C(p)*** is the vector *[x(p), y(p)]*, giving the x and y coordinates of the curve as a function of the p^{th} vertebra, and *R(p)* is the radius of curvature. Changes in geometric curvature at each vertebra along the sagittal plane of the spines were compared between prolonged paralysis or timed paralysis groups using one-way ANOVAs with a Tukey-HSD *post-hoc* test (95% confidence interval) (GraphPadPrism 4), with a p-value ≤ 0.05 taken as a statistically significant difference between groups. Data are expressed in the form of mean ± standard error of the mean (SEM).

Vertebral segmentation

Histological analysis of vertebral segmentation, the distinct spatial separation of cartilaginous vertebrae, was performed following paraffin embedding, sectioning (8μm) and staining with 0.025% alcian blue in 3% acetic acid (for cartilage) for 1 hour followed by 1% picro-sirus red (for collagen) for 1 hour.

Vertebral shape

Measurements were made of individual vertebral bodies, of functional spinal units (FSUs: two adjoining vertebrae and an intervertebral disc) and of spinal segments (multiple FSUs) of selected regions of the cervical (C10–C14), thoracic (T4–T7) and lumbar (L4-L7) spine. Virtual dissection and 2D measurements were performed in ImageJ. Vertebral body height, anterior to posterior vertebral sagittal width, and vertebral width from neural arch to neural arch were measured. The heights of individual FSUs and spinal segments were measured on mid-sagittal sections, with height defined as the distance from the superior endplate of one

vertebra to the inferior endplate of another. Triplicate technical replicates were generated through three mid-planar sections and the average measurements were compared between prolonged paralysis or timed paralysis groups using one-way ANOVAs with a Tukey-HSD *post-hoc* test (95% confidence interval) (SPSS Statistics 22.0) with a p-value ≤ 0.05 taken as a statistically significant difference. Wedging of vertebral bodies was quantified by measuring the angle made at the intersection of lines drawn along the superior and inferior endplate surfaces of an individual vertebra, as shown in Figure 3A.

RESULTS

Prolonged rigid paralysis vs. prolonged flaccid paralysis

A total of 66 rigidly paralyzed embryos, 12 flaccidly paralyzed embryos and 28 non-paralyzed controls were analyzed, as summarised in Table 1. There were pronounced sagittal curvature deformities in the chicks subjected to rigid paralysis, with multiple regions exhibiting distortion or bending, as compared to control spines (Figure 1B), and large variation between the individual curvatures (Supplementary Figure 1B). No dramatic curvature abnormalities were observed in the flaccidly paralyzed spines (Figure 1B). While there were no significant differences in geometric curvature between either the rigid and control groups or the flaccid and control groups (Figure 1C), there were significant differences in curvature between the rigid and flaccid groups at C8 and C9, with the rigid group showing more lordosis in the cervical region than the flaccid or control groups (Figure 1C). The lack of statistically significant differences between the rigid and control groups is likely to be due to the large variation in individual curvatures in the rigidly paralyzed group, as shown in Supplementary Figure 1B. No distinct alterations were identified in the coronal planes of either rigidly or flaccidly paralyzed spines (Supplementary Figure 2).

Histological analysis revealed that prolonged rigid paralysis led to abnormal cartilaginous separation posteriorly and anteriorly in the cervical region, with a continuous cartilaginous

posterior structure (fused spinous processes) and abnormal definition of the joint between vertebral bodies (symphysis joints), as shown in Figure 2B. Fusion of the posterior spinous processes was also present in the thoracic and lumbar regions of rigidly paralyzed spines, while the symphysis joints in these regions appeared to form normally, as shown in Supplementary Figure 3. No segmentation abnormalities were evident with flaccid paralysis, yet the morphologies of the spinous processes were abnormal in the cervical region (as shown in Figure 2B). The spinous processes of the thoracic and lumbar regions in flaccidly paralyzed specimens were similar to those of non-paralyzed controls. Histological analyses also revealed unusual pathological changes in the vertebrae of rigidly paralyzed spines, including distortions in the normal sagittal cross-sectional shape of the vertebral bodies in the cervical and thoracic regions (Supplementary Figure 4). A feature evident from visual inspection of the rigidly paralyzed spines is regions of extreme curvature (also visible in Figure 1B, Rigid) in which separation of the joints of vertebral bodies has taken place (Figure 3C ii & iv), while the spinal column remains intact through the posterior spinous process joints. Histological analysis revealed regions in which the spinal cord protrudes anteriorly, separating the vertebral bodies (as shown in Supplementary Figure 4i), and this is likely what is leading to these regions of extreme curvature.

Changes in size and shape of vertebral bodies and spinal segment shapes were quantified in sub-regions of the cervical, thoracic and lumbar spine (vertebrae of the sacral and caudal regions were not analyzed based on a lack of relevance to the human spine). When heights of individual and multiple FSUs in selected sub-regions were measured, no differences were found in any region for either paralysis group. However, analysis of individual vertebrae revealed that the vertebral body height of C10 was significantly reduced in both prolonged paralysis groups, with average reductions of 16.8% following rigid paralysis and 18.1% following flaccid paralysis (Figure 2C-E). No FSUs within which C10 was contained showed

changes in height, which could be due to the effects of wedging, as shown in Figure 3. The only other significant shape change found was an increase in vertebral sagittal width in T6 and T7 (by an average of 26.3% and 24.1%, respectively) in the rigidly paralyzed group (Figure 2D-E). Wedging was apparent in the thoracic region of the rigidly paralyzed spines, as illustrated in Figure 3. While control vertebral endplates were parallel (angle of zero degrees), all of the vertebrae within the T4 to T7 spinal segment exhibited posterior wedging, with average angles of 6.7±2.9° (T4), 7.2±2.0° (T5) 6.2±2.2° (T6) and 7.8±1.7° (T7) (Table 2). While it is likely that wedging also was present in the cervical spine of rigidly paralyzed spines, vertebral fusion in this region prevented measurement of wedging angles. No wedging was present in the flaccidly paralyzed spines (Table 2g).

Timed initiation of rigid paralysis

In addition to the prolonged rigid paralysis experiment (E3–E9) already described, five further rigid paralysis regimes were administered by varying the day of onset of paralysis from E4 to E8. The numbers of specimens analyzed are summarised in Table 1, with controls being pooled between groups. When rigid paralysis was initiated on or before E5, this resulted in multiple regions of abnormal kyphosis and lordosis compared to normal sagittal curvatures (Figure 4A). However, only paralysis from E4 led to significant differences in curvature as compared to controls, with significant changes in geometric curvature at five vertebral locations; C3, C4 and L5–L7 (Figure 4B). As in the case of prolonged rigid paralysis, the lack of statistically significant changes in geometric curvature in spines paralyzed on E5 or earlier is likely to be due to the large variation between individual specimens (Supplementary Figure 1). Commencing rigid paralysis on or after E6 did not have a measurable effect on curvature, with no distinct abnormalities in sagittal curvature evident from outlines (Figure 4A), and no significant differences in geometric curvature (Figure 4B). These results suggest that onset of rigid paralysis on or before E5, which is prior to formation of the vertebrae at E6[36], has the

most severe effects on development of general spinal curvature, with initiation of rigid paralysis at E4 leading to the most consistent effects on geometric curvature.

Histological analysis of the additional groups in which rigid paralysis was initiated on or before E5 exhibited similar results to those described for the prolonged rigid paralysis (E3–E9) group. All of these groups had fusion of the posterior spinous processes in the cervical, thoracic and lumbar regions (Figure 5A, Supplementary Figure 3), and fusion of the symphysis joints in the cervical region, with apparently normal segmentation of the symphysis joints in the thoracic and lumbar regions (Figure 5A, supplementary Figure 3). In all three of the groups paralyzed on or after E6, a collagen rich space was visible posteriorly and anteriorly between the vertebrae (Figure 5A), indicating normal segmentation of both the spinous processes and symphysis joints. As performed previously, changes in size and shape of vertebral bodies and spinal segment shapes were quantified in sub-regions of the cervical, thoracic and lumbar spine. As in the prolonged rigid paralysis results, no difference in FSU or spinal segment height was found in either of the additional groups paralyzed on or before E5. Similarly to the prolonged rigid paralysis group, there were reductions in the vertebral body height of C10, with average reductions of 19.3% for the E4–E9 group and 21.8% for the E5–E9 group (Figure 5B). The only other significant difference measured in these groups was a reduction in the vertebral body width of L5 by an average of 22% in the group that underwent paralysis from E4–E9 (Figure 5C). The only shape difference found in the groups paralyzed from E6 onwards was a reduction in the vertebral width of T6 by 18.8% in the E7–E9 group (Figure 5D). Average posterior wedging angles in T4–T7 varied from 6–7º for the E3–E9 group (as previously described), 3–5º for the E4–E9 and E5–E9 groups, 2–3º for the E6–E9 group and less than 1º for the E7–E9 and E8–E9 groups, as summarized in Table 2. Therefore, the longer paralysis was maintained, the more severe the average posterior wedging angles.

DISCUSSION

Our primary hypothesis, that altering fetal movement causes abnormalities in the developing spine has been corroborated. Rigidly paralyzed spines showed distinct defects in all three of the key variables; curvature, segmentation and vertebral shape, while flaccidly paralyzed spines exhibited only subtle changes in vertebral shape, with no effects on curvature or segmentation. These results suggest that sustained, static muscle loading is highly detrimental to early spine development, while the removal of both static and dynamic components of muscle activity has mild effects on spine development at the single timepoint examined. The timing of initiation of rigid paralysis had a distinct influence on the extent of the effects on the spine, corroborating our secondary hypothesis that paralysis at earlier stages of development would result in more severe spinal deformations. Spines subjected to initiation of rigid paralysis on or before E5 were severely affected with curvature and segmentation abnormalities, while the only measureable differences to controls in spines of specimens paralyzed from E6 onwards were slight wedging angles, and a change in one shape parameter in one of the sub-groups.

There are some limitations to this research. As all of our analyses were performed at E9, we do not know how segmentation, shape morphogenesis and spinal curvature are affected prior to, or after this timepoint. For example, although prolonged flaccid paralysis did not lead to dramatic effects on the spine at E9, it is possible that had development been allowed to progress further, more pronounced effects would have emerged. Such investigations will be undertaken in future studies. The prolonged paralysis regimes used in this study are well-controlled and prioritise the identification of effects, but would be extreme compared to what might occur in a clinical condition of reduced or abnormal fetal movement. However, the prolonged paralysis regimes would be analogous to fetal akinesia deformation sequence (FADS)[9,10], and the timed studies illustrate that even short periods of immobility can have local effects on vertebral shape and wedging angles. Finally, since the chick notochord does not undergo involution and since

the disc lacks a nucleus pulposus, this study does not characterise the effects of paralysis on the intervertebral disc, and a mammalian model system of abnormal fetal movements would be necessary to investigate the disc. Nonetheless, many aspects of the current study have only have been possible due to the flexibility of the chick system, and investigation of the effects of timed paralysis in a mammalian system would be very difficult, if not impossible.

Aspects of abnormal spine development identified in this study correlate with the key features of congenital spine deformities, namely curvature abnormalities and vertebral wedging. Initiation of rigid paralysis on or before E5 induced severe effects on spinal curvature, with regions of hyper-lordosis and hyper-kyphosis, as seen, respectively, in congenital lordosis and kyphosis[2]. Vertebral body wedging was evident in the thoracic region following rigid paralysis, which, in the case of scoliosis, has been shown to correlate with the severity of curvature defect[37,38]. While curvature changes in the coronal plane are the most common presentation of congenital spine deformities[1] (which, however, are commonly associated with a sagittal deformity[2]) no changes in coronal curvature were seen in the model system. This difference could be due to the pronounced differences in spinal anatomy of the chicken and human, and could also be related to the differences in developmental mechanical environments of the mammal and bird. Future work will explore use of a mammalian model system of abnormal fetal movements to provide insight into this aspect.

While there is very sparse literature from animal models with which to compare our results, alternations in spinal curvature have previously been reported, but not quantified, in immobilized chicks under prolonged paralysis[24-26], and in mammalian models of absent fetal movements[20,28,39]. Fusion of the vertebrae has also been previously reported in animal models of abnormal fetal movements[20,24,25,27,28], but this study is the first to describe region-specific fusion, both in the description of fusion of posterior and anterior aspects of the vertebrae (spinous processes vs. symphysis joints), and the identification of the cervical spine as the part

of the spine most prone to vertebral fusions following prolonged rigid paralysis. Furthermore, this is the first study to look at the effects of varying the time of onset of paralysis on the spine, and the only study to describe the effects of flaccid paralysis on the spine.

A number of aspects of the results merit further discussion. For all of the experiments described, global paralysis led to local effects, with some regions being more affected than others. With both types of prolonged paralysis, the cervical spine was the most affected region, with shape changes in C10, and significant differences in curvature in C8 and C9 between the paralyzed groups. In the prolonged and early (on or before E5) rigidly paralyzed groups, only the cervical region had abnormal segmentation for both the anterior symphysis joints and the posterior spinous process joints while in the prolonged flaccid group, the spinous process joints of only the cervical region were abnormally shaped. Considering the very long length of the cervical spine in the chick (Figure 1), and the large size of the chick head at early stages of development, it is possible that the weight of the head exacerbates the effects of paralysis. Since the human cervical spine has much fewer vertebrae than in the chick, the cervical region may not be disproportionately affected during human development. It is unclear why the shape of C10 was particularly prone to shape changes. C10 falls within the normal kyphotic curve of the cervical spine, which could potentially lead to a higher likelihood of deformation of this region. Commencing rigid paralysis on or prior to E6 led to substantial (>1°) wedging in the thoracic spine. Rib cartilage appears in the chick from E7–7.5[36], and alterations in the development of ribs have previously been reported following a reduction in mechanical stimulation[39,40]. Therefore, the alterations seen in the thoracic region may be due to an alteration in rib architecture, which will be investigated in future studies. Finally, this study quantified shape changes in sub-regions of the cervical, thoracic and lumbar spine. Even within the regions in which changes in curvature occurred, the shape parameters measured (vertebral body height, sagittal width and anterior width) were not significantly different from the

342 equivalent measurements in non-paralyzed controls. Since our analyses were performed at a
343 single timepoint, it is possible that vertebral shape abnormalities prior to E9 could lead to
344 changes in curvature in other regions of the spine as development progresses.

345 With rigid paralysis, only the dynamic component of the muscle forces is absent and sustained
346 static loading is applied, while with flaccid paralysis, both the rigid and static components are
347 absent. In the joints of the chick limb, rigid paralysis has been shown to have slightly more
348 pronounced effects on the length and breadth of the cartilaginous epiphyses than flaccid
349 paralysis[31], while conversely, late application of rigid paralysis induced more normal cavitation
350 of the joints of the limb as compared to late flaccid paralysis[31]. The current study shows that
351 the effects on the spine of prolonged rigid paralysis are dramatic, while the effects of prolonged
352 flaccid paralysis are more subtle. Our working hypothesis is that the structures of the very early
353 spinal column are malleable, leading to their deformation under sustained static loading (rigid
354 paralysis). It has previously been proposed that static loading supresses cartilaginous growth
355 in the rudiments of the limbs[31], and we believe that this is what occurs in the spine. This theory
356 is bolstered by the fact that the very small, delicate joints of the spinous processes are more
357 widely affected than the thicker joints of the vertebral bodies in rigidly paralyzed spines.
358 Although the effects of rigid paralysis were more dramatic, prolonged flaccid paralysis did
359 have some effects on the shape of some spinous processes and on the shape of one vertebral
360 body, which could become more pronounced over subsequent development. Another key novel
361 finding of this study is the apparent "cut-off" timepoint of E6, where rigid paralysis from E5
362 or earlier leads to abnormal curvatures and vertebral segmentation, while paralysis after E6 did
363 not affect curvature or vertebral segmentation. E3 marks the developmental timepoint at which
364 a well-defined myotome is present in the developing chick[36], while movement of the embryonic
365 chick neck and spine has been reported to start at E3.5[41]. Formation of the sclerotome, from
366 which the vertebral bodies and spinous processes form, begins at around E2.5, but the

segmentation of distinct cartilaginous vertebrae is not complete until E6[36,42] (all timings for the chick embryo). These results therefore indicate that sustained, static loading is particularly detrimental to the process of sclerotome development during which it is sub-compartmentalized to form the different parts of the axial skeleton, most likely due to compression of the emerging, delicate structures.

In conclusion, this study demonstrates that both the timing and the type of mechanical stimulation due to fetal movements are key to a number of aspects of the developing spine, including spinal curvature and vertebral segmentation and shape, with important implications for future research into the aetiology of congenital spine deformities.

ACKNOWLEDGEMENTS

This research was funded by a Leverhulme Trust Research Project Grant (RPG-2014-339).

REFERENCES

1 Burnei, G. *et al.* Congenital scoliosis: an up-to-date. *Journal of medicine and life* **8**, 388-397 (2015).

2 Lonstein, J. E. Congenital spine deformities: scoliosis, kyphosis, and lordosis. *The Orthopedic clinics of North America* **30**, 387-405, viii (1999).

3 McMaster, M. J. & Singh, H. Natural history of congenital kyphosis and kyphoscoliosis. A study of one hundred and twelve patients. *The Journal of bone and joint surgery. American volume* **81**, 1367-1383 (1999).

4 Batra, S. & Ahuja, S. Congenital scoliosis: management and future directions. *Acta orthopaedica Belgica* **74**, 147-160 (2008).

5 Giampietro, P. F. *et al.* Clinical, genetic and environmental factors associated with congenital vertebral malformations. *Molecular syndromology* **4**, 94-105, doi:10.1159/000345329 (2013).

6 Li, Z. *et al.* Vitamin A deficiency induces congenital spinal deformities in rats. *PloS one* **7**, e46565, doi:10.1371/journal.pone.0046565 (2012).

7 Sparrow, D. B. *et al.* A mechanism for gene-environment interaction in the etiology of congenital scoliosis. *Cell* **149**, 295-306, doi:10.1016/j.cell.2012.02.054 (2012).
8 Loder, R. T. *et al.* The induction of congenital spinal deformities in mice by maternal carbon monoxide exposure. *Journal of pediatric orthopedics* **20**, 662-666 (2000).
9 Moessinger, A. C. Fetal akinesia deformation sequence: an animal model. *Pediatrics* **72**, 857-863 (1983).
10 Hall, J. G. Pena-Shokeir phenotype (fetal akinesia deformation sequence) revisited. *Birth defects research. Part A, Clinical and molecular teratology* **85**, 677-694, doi:10.1002/bdra.20611 (2009).
11 Bisceglia, M., Zelante, L., Bosman, C., Cera, R. & Dallapiccola, B. Pathologic features in two siblings with the Pena-Shokeir I syndrome. *European journal of pediatrics* **146**, 283-287 (1987).
12 Crane, J. P. & Heise, R. L. New syndrome in three affected siblings. *Pediatrics* **68**, 235-237 (1981).
13 Elias, S., Boelen, L. & Simpson, J. L. Syndromes of camptodactyly, multiple ankylosis, facial anomalies, and pulmonary hypoplasia. *Birth defects original article series* **14**, 243-251 (1978).
14 Lazjuk, G. I., Cherstvoy, E. D., Lurie, I. W. & Nedzved, M. K. Pulmonary hypoplasia, multiple ankyloses, and camptodactyly: one syndrome or some related forms? *Helvetica paediatrica acta* **33**, 73-79 (1978).
15 Lindhout, D. *et al.* The Pena-Shokeir syndrome: report of nine Dutch cases. *American journal of medical genetics* **21**, 655-668, doi:10.1002/ajmg.1320210407 (1985).
16 Mailhes, J. B., Lancaster, K., Bourgeois, M. J. & Sanusi, I. D. 'Pena-Shokeir syndrome' in a newborn male infant. *American journal of diseases of children (1960)* **131**, 1419-1420 (1977).
17 Ochi, H., Kobayashi, E., Matsubara, K., Katayama, T. & Ito, M. Prenatal sonographic diagnosis of Pena-Shokeir syndrome type I. *Ultrasound in obstetrics & gynecology : the official journal of the International Society of Ultrasound in Obstetrics and Gynecology* **17**, 546-547, doi:10.1046/j.1469-0705.2001.00405.x (2001).
18 Stokes, I. A., Burwell, R. G. & Dangerfield, P. H. Biomechanical spinal growth modulation and progressive adolescent scoliosis--a test of the 'vicious cycle' pathogenetic hypothesis: summary of an electronic focus group debate of the IBSE. *Scoliosis* **1**, 16, doi:10.1186/1748-7161-1-16 (2006).

19 Nowlan, N. C., Murphy, P. & Prendergast, P. J. Mechanobiology of embryonic limb development. *Annals of the New York Academy of Sciences* **1101**, 389-411, doi:10.1196/annals.1389.003 (2007).

20 Kahn, J. *et al.* Muscle contraction is necessary to maintain joint progenitor cell fate. *Developmental cell* **16**, 734-743, doi:10.1016/j.devcel.2009.04.013 (2009).

21 Nowlan, N. C. *et al.* Developing bones are differentially affected by compromised skeletal muscle formation. *Bone* **46**, 1275-1285, doi:10.1016/j.bone.2009.11.026 (2010).

22 Nowlan, N. C., Chandaria, V. & Sharpe, J. Immobilized chicks as a model system for early-onset developmental dysplasia of the hip. *Journal of orthopaedic research : official publication of the Orthopaedic Research Society* **32**, 777-785, doi:10.1002/jor.22606 (2014).

23 Roddy, K. A., Prendergast, P. J. & Murphy, P. Mechanical influences on morphogenesis of the knee joint revealed through morphological, molecular and computational analysis of immobilised embryos. *PloS one* **6**, e17526, doi:10.1371/journal.pone.0017526 (2011).

24 Murray, P. D. & Drachman, D. B. The role of movement in the development of joints and related structures: the head and neck in the chick embryo. *Journal of embryology and experimental morphology* **22**, 349-371 (1969).

25 Sullivan, G. Prolonged paralysis of the chick embryo, with special reference to effects on the vertebral column. *Australian Journal of Zoology* **14**, 1-17, doi:http://dx.doi.org/10.1071/ZO9660001 (1966).

26 Sullivan, G. Skeletal abnormalities in chick embryos paralysed with decamethonium. *Australian Journal of Zoology* **22**, 429-438, doi:http://dx.doi.org/10.1071/ZO9740429 (1974).

27 Hosseini, A. & Hogg, D. A. The effects of paralysis on skeletal development in the chick embryo. I. General effects. *Journal of anatomy* **177**, 159-168 (1991).

28 Rot-Nikcevic, I. *et al.* Myf5-/- :MyoD-/- amyogenic fetuses reveal the importance of early contraction and static loading by striated muscle in mouse skeletogenesis. *Development genes and evolution* **216**, 1-9, doi:10.1007/s00427-005-0024-9 (2006).

29 Kaplan, K. M., Spivak, J. M. & Bendo, J. A. Embryology of the spine and associated congenital abnormalities. *The spine journal : official journal of the North American Spine Society* **5**, 564-576, doi:10.1016/j.spinee.2004.10.044 (2005).

30 Bruggeman, B. J. *et al.* Avian intervertebral disc arises from rostral sclerotome and lacks a nucleus pulposus: implications for evolution of the vertebrate disc. *Developmental dynamics : an official publication of the American Association of Anatomists* **241**, 675-683, doi:10.1002/dvdy.23750 (2012).

31 Osborne, A. C., Lamb, K. J., Lewthwaite, J. C., Dowthwaite, G. P. & Pitsillides, A. A. Short-term rigid and flaccid paralyses diminish growth of embryonic chick limbs and abrogate joint cavity formation but differentially preserve pre-cavitated joints. *Journal of musculoskeletal & neuronal interactions* **2**, 448-456 (2002).

32 Reiser, P. J., Stokes, B. T. & Walters, P. J. Effects of immobilization on the isometric contractile properties of embryonic avian skeletal muscle. *Experimental neurology* **99**, 59-72 (1988).

33 Sharpe, J. *et al.* Optical projection tomography as a tool for 3D microscopy and gene expression studies. *Science (New York, N.Y.)* **296**, 541-545, doi:10.1126/science.1068206 (2002).

34 Schneider, C. A., Rasband, W. S. & Eliceiri, K. W. NIH Image to ImageJ: 25 years of image analysis. *Nature methods* **9**, 671-675 (2012).

35 Vrtovec, T., Likar, B. & Pernus, F. Quantitative analysis of spinal curvature in 3D: application to CT images of normal spine. *Physics in medicine and biology* **53**, 1895-1908, doi:10.1088/0031-9155/53/7/006 (2008).

36 Shapiro, F. Vertebral development of the chick embryo during days 3-19 of incubation. *Journal of morphology* **213**, 317-333, doi:10.1002/jmor.1052130305 (1992).

37 Braun, J. T. *et al.* Experimental scoliosis in an immature goat model: a method that creates idiopathic-type deformity with minimal violation of the spinal elements along the curve. *Spine* **28**, 2198-2203, doi:10.1097/01.brs.0000085095.37311.46 (2003).

38 Perdriolle, R., Becchetti, S., Vidal, J. & Lopez, P. Mechanical process and growth cartilages. Essential factors in the progression of scoliosis. *Spine* **18**, 343-349 (1993).

39 Pai, A. C. Developmental Genetics of a Lethal Mutation, Muscular dysgenesis (MGD),in the mouse. I. Genetaic analysis and gross morphology. . *Developmental biology* **11**, 82-92 (1965).

40 Hall, B. K. & Herring, S. W. Paralysis and growth of the musculoskeletal system in the embryonic chick. *Journal of morphology* **206**, 45-56, doi:10.1002/jmor.1052060105 (1990).

41 Hamburger, V. & Balaban, M. Observations and experiments on spontaneous rhythmical behavior in the chick embryo. *Developmental biology* **6**, 533-545 (1963).

42 Scaal, M. Early development of the vertebral column. *Seminars in cell & developmental biology*, doi:10.1016/j.semcdb.2015.11.003 (2015).

TABLES AND FIGURE LEGENDS

Table 1: Numbers of paralyzed and non-paralyzed chick embryos harvested at embryonic day (E) 9.

Table 2: Average posterior vertebral wedge angles for thoracic vertebrae T4–T7 for control (h) and paralyzed groups (a-g). Measurements shown in degrees. SD; standard deviation.

Figure 1: Rigid paralysis induced more severe abnormalities in curvature than flaccid paralysis. (**A**) E9 chick whole spine stained for cartilage. P; posterior, A; Anterior. (**B**) Overlays of curvatures in the sagittal plane of control spines (blue, n=21), prolonged flaccidly paralyzed spines (orange, n=7) and prolonged rigidly paralyzed spines (red, n=8), with all spines aligned to thoracic vertebra 1 (T1). Regions of pronounced abnormal lordosis (green arrows) and kyphosis (purple stars) are highlighted. Scale Bars 2000μm. (**C**) Geometric curvature (GC) analysis of flaccidly paralyzed spines (orange line, n=7), rigid paralyzed spines (red line, n=8) and control curves (blue line, n=21). Y-axis; 1/ radius of curvature, represented by arbitrary units of length. GC>0 lordotic curve, GC<0 kyphotic curve, GC=0 straight spine. X-axis; the craniocaudal individual vertebrae. Significant differences were identified between paralysis regimes at C8 and C9, * $p \leq 0.05$. C; cervical, T; thoracic, L; lumbar, S; sacral.

Figure 2: Prolonged rigid paralysis induced vertebral cartilaginous fusion while both prolonged paralysis regimes led to a reduction in vertebral body height in C10. Prolonged rigid paralysis also led to a decrease in the vertebral sagittal width of T6 and T7. (**A**) Schematic of a normal sagittal cross section of a portion of the cervical region indicating clear separation of the spinous process (sp) and the symphysis joints (SJ). (**B**) Sagittal sections stained with alcian blue (for cartilage) and picrosirus red (for collagen) show posterior spinous process (i, iii, v)

and anterior symphysis joints (ii, iv, vi) in control (i-ii), flaccidly (iii-iv) and rigidly paralyzed (v-vi) spines in the cervical region. Posterior vertebral fusion of the spinous processes (sp) is indicated by the continuous cartilaginous staining (green arrow) and fusion of the symphysis joints (SJ) (orange arrow). Scale bars100µm. P; posterior, A; anterior. (**C**) Representative sagittal 3D views of cervical spine segment (C10–C14) and ventral, sagittal and axial 3D views of C10 from control, prolonged flaccid and prolonged rigid paralysis. Yellow lines and asterisks in ventral view indicate the significant reduction in vertebral body (VB) height of C10 with flaccid and rigid paralysis compared to controls. (**D**) Representative sagittal 3D views of thoracic spine segment (T4–T7) and ventral, sagittal and axial 3D views of T6 and T7 from control and prolonged rigid paralysis. Yellow lines and asterisks in sagittal view indicate the significant increase in vertebral sagittal width in T6 and T7 with prolonged rigid paralysis compared to controls. Scale bar 1000µm. (**E**) Box plots showing significant reductions in VB height of C10 and increases in the sagittal width of T6 and T7 following prolonged rigid paralysis. * $p \leq 0.05$.

Figure 3: Prolonged rigid paralysis led to vertebral wedging in the thoracic region. (**A**) Representative sagittal 3D view of thoracic spine segment (T4-T7) of control and rigidly paralyzed specimens. Yellow lines in each case show how the vertebral body angle measurements were created. (**B**) Schematic view of thoracic spinal segments in (A) illustrating the differences in vertebral wedging and separation of vertebrae. (**C**) Individual spines from 5 distinct chicks (i-v) paralyzed rigidly from E3–E9 showing evidence of vertebral wedging in the thoracic region (grey boxes). In regions of extreme curvature (indicated by arrow heads), separation at the anterior vertebral body joints occurs while the posterior spinous process joints remain intact. Scale bar 2000µm.

Figure 4: Initiation of rigid paralysis on or prior to E5 led to reversals and exaggerations of curvature, while paralysis from E4 led to significant alterations in curvatures in five discrete locations. (**A**) Overlays of curvatures in sagittal plane of control spines (blue, n=21), and timed paralysis spines (E3–E9: red, n=8; E4–E9: brown, n=10; E5–E9: green, n=9; E6–E9: purple, n=8; E7–E9: grey, n=6; E8–E9: mustard, n=5). All spines aligned to thoracic vertebra 1 (T1). Regions of pronounced abnormal lordosis (green arrows) and kyphosis (purple stars) are highlighted. Scale Bars 2000μm. P; posterior, A; Anterior. (**B**) GC analysis of each group. Y-axis; 1/ radius of curvature, represented by arbitrary units of length. GC>0 lordotic curve, GC<0 kyphotic curve, GC=0 straight spine. X-axis; the craniocaudal individual vertebrae. Significant differences in curvature were found in spines paralyzed from E4-E9, * $p \leq 0.05$, ** $p \leq 0.01$. C; cervical, T; thoracic, L; lumbar, S; sacral, Cd; caudal.

Figure 5: Initiation of rigid paralysis on or prior to E5 induced posterior vertebral cartilaginous fusion and discrete changes in vertebral shape, while paralysis on or after E6 showed normal segmentation but discrete shape changes in the thoracic region. (**A**) Sagittal alcian blue (cartilage) and picro–sirus red (collagen) stained sections of posterior spinous process (i, iii, v, vii, ix, xi, xiii) and anterior symphysis joints (ii, iv, vi, viii, x, xii, xiv) in control (i-ii) and timed rigid paralysis spines in the cervical region. Posterior vertebral fusion of the spinous process (sp) is indicated by the continuous cartilaginous staining (green arrows) as is fusion of the symphysis joints (SJ) (orange arrow). Scale bars100μm. P; posterior, A; anterior. (**B**) Representative sagittal 3D views of cervical spine segment (C10-C14) and ventral, sagittal and axial 3D views of C10 from control and rigid (E4–E9, E5-E9) paralysis groups. (**C**) Representative sagittal 3D views of lumbar spine segment (L4-L7) and ventral, sagittal and axial 3D views of L5 from control and rigid (E4-E9) paralysis groups. (**D**) Representative sagittal 3D views of thoracic spine segment (T4–T7) and ventral, sagittal and axial 3D views

of T6 from control, rigid (E7–E9) paralysis. (**B-D**) Yellow lines indicate the significant differences with paralysis compared to controls. Scale bar 1000µm.

Supplementary Figure 1: Individual curvatures in the sagittal plane of (**B–D**) spines paralyzed on or prior to E5 compared to (**A**) control curvatures aligned to thoracic vertebra 1 (T1). Variation in control curvatures is evident, with more pronounced variation in the cervical and caudal regions depending on the position of the head, and the position of the embryonic pygostyle (plate of bone at the posterior end of the spine). Lordotic (green arrows) and kyphotic (purple stars) curvatures resulted from rigid paralysis, with more severe alterations observed in various sub-regions (**B**) from E3-E9, (**C**) E4-E9 and (**D**) E5-E9 paralyzed spines. Scale bars 2000µm

Supplementary Figure 2: Paralysis induced no pronounced changes in curvatures in the coronal plane. Overlays of curvatures in the coronal plane of control spines (n=21), prolonged flaccidly paralyzed spines (n=7), and rigidly paralyzed spines (E3–E9: n=8; E4–E9: n=10; E5–E9: n=9; E6–E9: n=8; E7–E9: n=6; E8–E9: n=5). All spines aligned to thoracic vertebra 1 (T1). Scale bars 2000µm.

Supplementary Figure 3: Comprehensive histological analysis of vertebral segmentation in E9 spines following (b, j, r) flaccid paralysis and (c–h, k–p, s–x) rigid paralysis from multiple initiation time-points compared to controls (a, i, q). Sections stained with alcian Blue- cartilage/ picro-sirus red- collagen. sc: spinal cord, n; notochord. P; posterior, A; anterior. Scale bars 100µm.

Supplementary Figure 4: Pathological changes in the vertebrae were observed following rigid paralysis commenced on or before E5. Dorsal (a–b) and lateral (c–d) views of paralyzed vertebrae show further evidence of vertebral fusion. (b’ and d’) are corresponding red boxes shown at higher magnifications. (f–g, red arrows) Distortions in normal sagittal cross-sectional shape of the vertebral bodies (vb) compared to (e) controls. A unique bending and anterior protrusion of the spinal cord (sc) was observed in one rigidly paralyzed specimen (i, orange arrow) compared to control (h) in which the spinal cord is enclosed within the vertebrae. Sp; spinous process, n; notochord, Scale bar in (a) 500µm, (b–i) 100µm.

Table 1: Numbers of paralyzed and non-paralyzed chick embryos harvested at embryonic day (E) 9.

	Non-paralyzed controls	Paralyzed						
		Rigid						Flaccid
Total	28	66						12
		E3–E9	**E4–E9**	**E5–E9**	**E6–E9**	**E7–E9**	**E8–E9**	**E3–E9**
3D	21	8	10	9	8	6	5	7
Histology	7	5	4	3	3	3	2	5

Table 2: Average posterior vertebral wedge angles for thoracic vertebrae T4–T7 for control (h) and paralyzed groups (a-g). Measurements shown in degrees. SD; standard deviation.

(a) Rigid Paralysis E3-E9		
	Average	SD
T4	6.72º	2.87
T5	7.24º	1.96
T6	6.19º	2.16
T7	7.82º	1.66

(b) Rigid Paralysis E4-E9		
	Average	SD
T4	4.29º	1.67
T5	4.79º	2.74
T6	3.96º	2.20
T7	3.60º	2.17

(c) Rigid Paralysis E5-E9		
	Average	SD
T4	3.09º	1.35
T5	3.95º	2.53
T6	3.68º	2.05
T7	3.16º	2.38

(d) Rigid Paralysis E6-E9		
	Average	SD
T4	2.34 º	1.94
T5	2.27 º	1.46
T6	2.65 º	1.92
T7	2.40 º	1.07

(e) Rigid Paralysis E7-E9		
	Average	SD
T4	0.26º	0.41
T5	0.23º	0.37
T6	0.45º	0.62
T7	0.77º	1.05

(f) Rigid Paralysis E8-E9		
	Average	SD
T4	0.40 º	0.90
T5	0.40 º	0.90
T6	0º	0
T7	0º	0

(g) Flaccid Paralysis E3-E9		
	Average	SD
T4	0º	0
T5	0º	0
T6	0º	0
T7	0º	0

(h) Non Paralyzed Controls		
	Average	SD
T4	0º	0
T5	0º	0
T6	0º	0
T7	0º	0

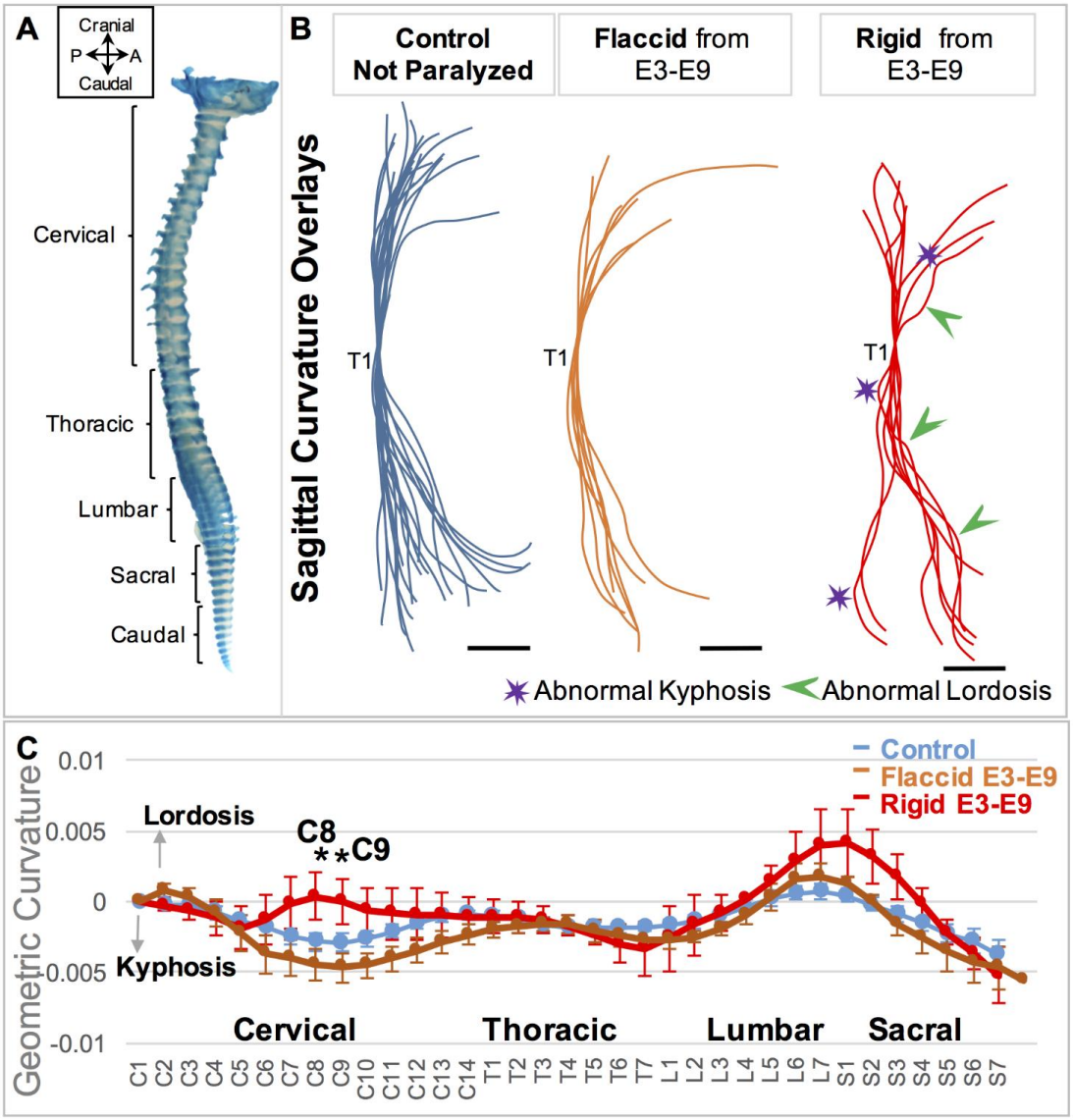

Figure 1: Rigid paralysis induced more severe abnormalities in curvature than flaccid paralysis. (**A**) E9 chick whole spine stained for cartilage. P; posterior, A; Anterior. (**B**) Overlays of curvatures in the sagittal plane of control spines (blue, n=21), prolonged flaccidly paralyzed spines (orange, n=7) and prolonged rigidly paralyzed spines (red, n=8), with all spines aligned to thoracic vertebra 1 (T1). Regions of pronounced abnormal lordosis (green arrows) and kyphosis (purple stars) are highlighted. Scale Bars 2000µm. (**C**) Geometric curvature (GC) analysis of flaccidly paralyzed spines (orange line, n=7), rigid paralyzed spines (red line, n=8) and control curves (blue line, n=21). Y-axis; 1/ radius of curvature, represented by arbitrary units of length. GC>0 lordotic curve, GC<0 kyphotic curve, GC=0 straight spine. X-axis; the craniocaudal individual vertebrae. Significant differences were identified between paralysis regimes at C8 and C9, * $p \leq 0.05$. C; cervical, T; thoracic, L; lumbar, S; sacral.

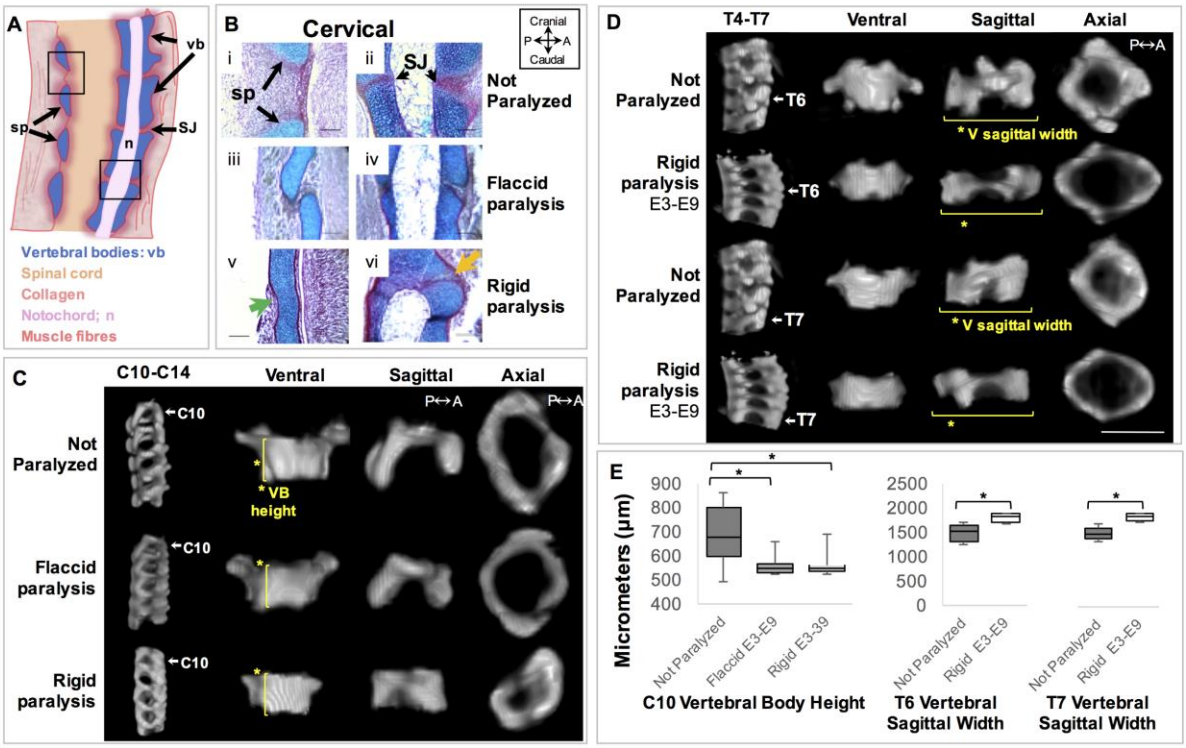

Figure 2: Prolonged rigid paralysis induced vertebral cartilaginous fusion while both prolonged paralysis regimes led to a reduction in vertebral body height in C10. Prolonged rigid paralysis also led to a decrease in the vertebral sagittal width of T6 and T7. (**A**) Schematic of a normal sagittal cross section of a portion of the cervical region indicating clear separation of the spinous process (sp) and the symphysis joints (SJ). (**B**) Sagittal sections stained with alcian blue (for cartilage) and picrosirus red (for collagen) show posterior spinous process (i, iii, v) and anterior symphysis joints (ii, iv, vi) in control (i-ii), flaccidly (iii-iv) and rigidly paralyzed (v-vi) spines in the cervical region. Posterior vertebral fusion of the spinous processes (sp) is indicated by the continuous cartilaginous staining (green arrow) and fusion of the symphysis joints (SJ) (orange arrow). Scale bars100µm. P; posterior, A; anterior. (**C**) Representative sagittal 3D views of cervical spine segment (C10–C14) and ventral, sagittal and axial 3D views of C10 from control, prolonged flaccid and prolonged rigid paralysis. Yellow lines and asterisks in ventral view indicate the significant reduction in vertebral body (VB) height of C10 with flaccid and rigid paralysis compared to controls. (**D**) Representative sagittal 3D views of thoracic spine segment (T4–T7) and ventral, sagittal and axial 3D views of T6 and T7 from control and prolonged rigid paralysis. Yellow lines and asterisks in sagittal view indicate the significant increase in vertebral sagittal width in T6 and T7 with prolonged rigid paralysis compared to controls. Scale bar 1000µm. (**E**) Box plots showing significant reductions in VB height of C10 and increases in the sagittal width of T6 and T7 following prolonged rigid paralysis. * p≤0.05.

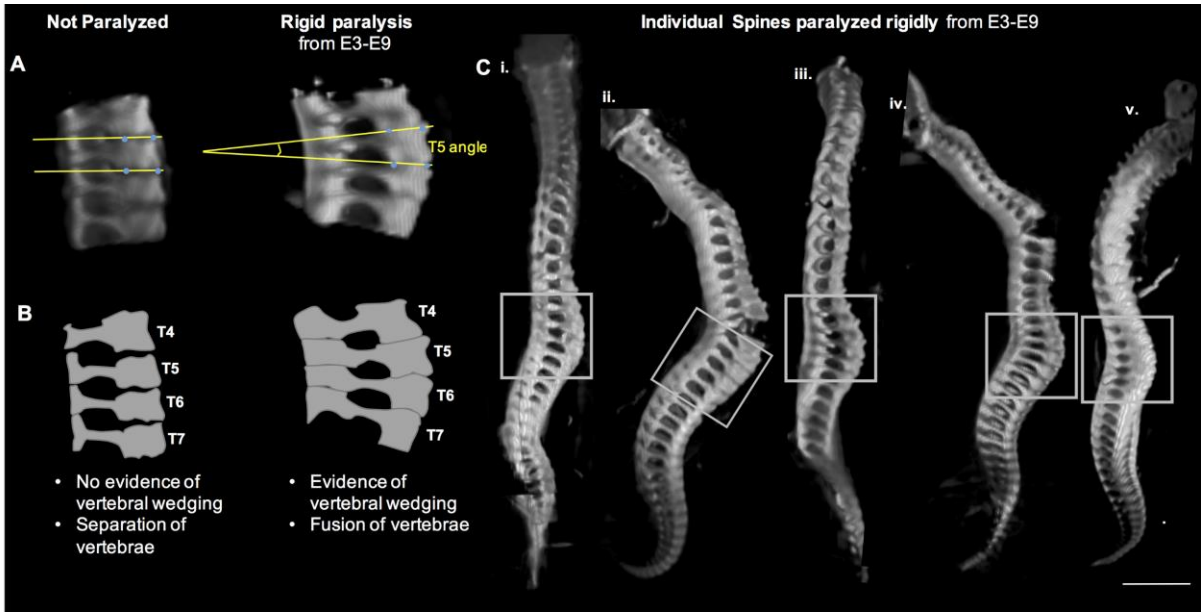

Figure 3: Prolonged rigid paralysis led to vertebral wedging in the thoracic region. (**A**) Representative sagittal 3D view of thoracic spine segment (T4-T7) of control and rigidly paralyzed specimens. Yellow lines in each case show how the vertebral body angle measurements were created. (**B**) Schematic view of thoracic spinal segments in (A) illustrating the differences in vertebral wedging and separation of vertebrae. (**C**) Individual spines from 5 distinct chicks (i-v) paralyzed rigidly from E3–E9 showing evidence of vertebral wedging in the thoracic region (grey boxes). In regions of extreme curvature (indicated by arrow heads), separation at the anterior vertebral body joints occurs while the posterior spinous process joints remain intact. Scale bar 2000µm.

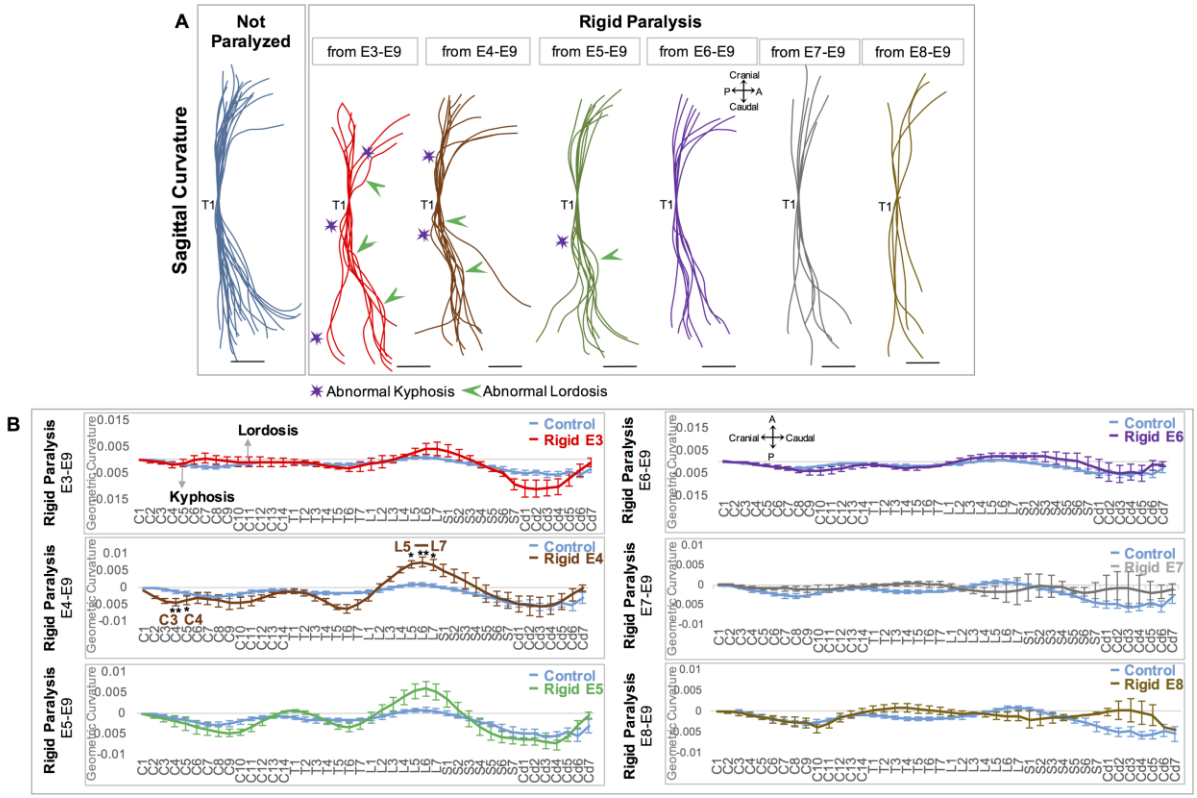

Figure 4: Initiation of rigid paralysis on or prior to E5 led to reversals and exaggerations of curvature, while paralysis from E4 led to significant alterations in curvatures in five discrete locations. (**A**) Overlays of curvatures in sagittal plane of control spines (blue, n=21), and timed paralysis spines (E3–E9: red, n=8; E4–E9: brown, n=10; E5–E9: green, n=9; E6–E9: purple, n=8; E7–E9: grey, n=6; E8–E9: mustard, n=5). All spines aligned to thoracic vertebra 1 (T1). Regions of pronounced abnormal lordosis (green arrows) and kyphosis (purple stars) are highlighted. Scale Bars 2000µm. P; posterior, A; Anterior. (**B**) GC analysis of each group. Y-axis; 1/ radius of curvature, represented by arbitrary units of length. GC>0 lordotic curve, GC<0 kyphotic curve, GC=0 straight spine. X-axis; the craniocaudal individual vertebrae. Significant differences in curvature were found in spines paralyzed from E4-E9, * $p \leq 0.05$, ** $p \leq 0.01$. C; cervical, T; thoracic, L; lumbar, S; sacral, Cd; caudal.

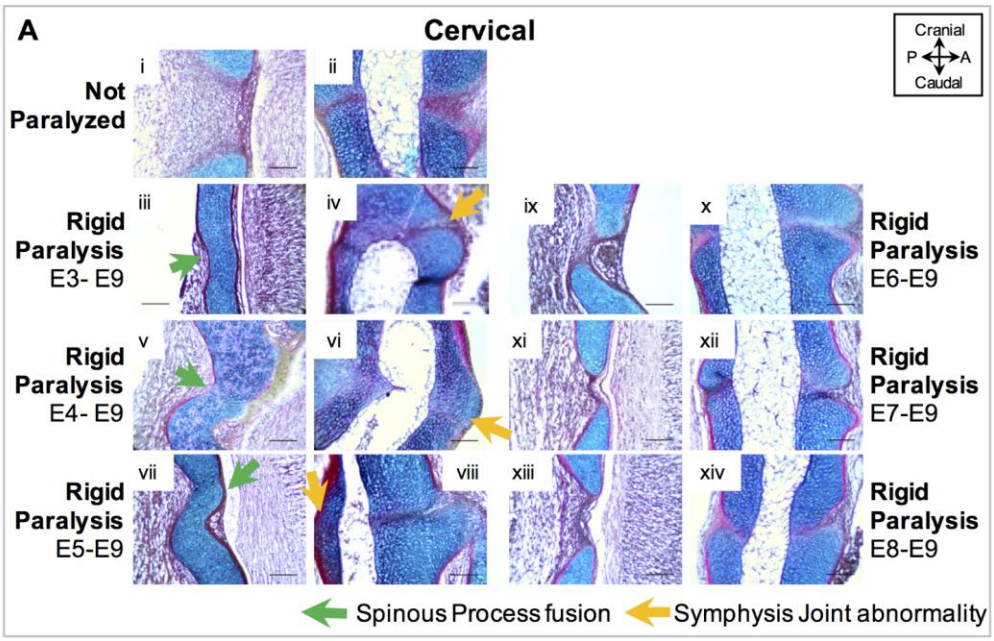
A
Cervical
Cranial
P
A
Caudal
Not Paralyzed
i
ii
Rigid Paralysis E3- E9
iii
iv
Rigid Paralysis E4- E9
v
vi
Rigid Paralysis E5-E9
vii
viii
ix
Rigid Paralysis E6-E9
x
Rigid Paralysis E7-E9
xi
xii
Rigid Paralysis E8-E9
xiii
xiv
Spinous Process fusion
Symphysis Joint abnormality

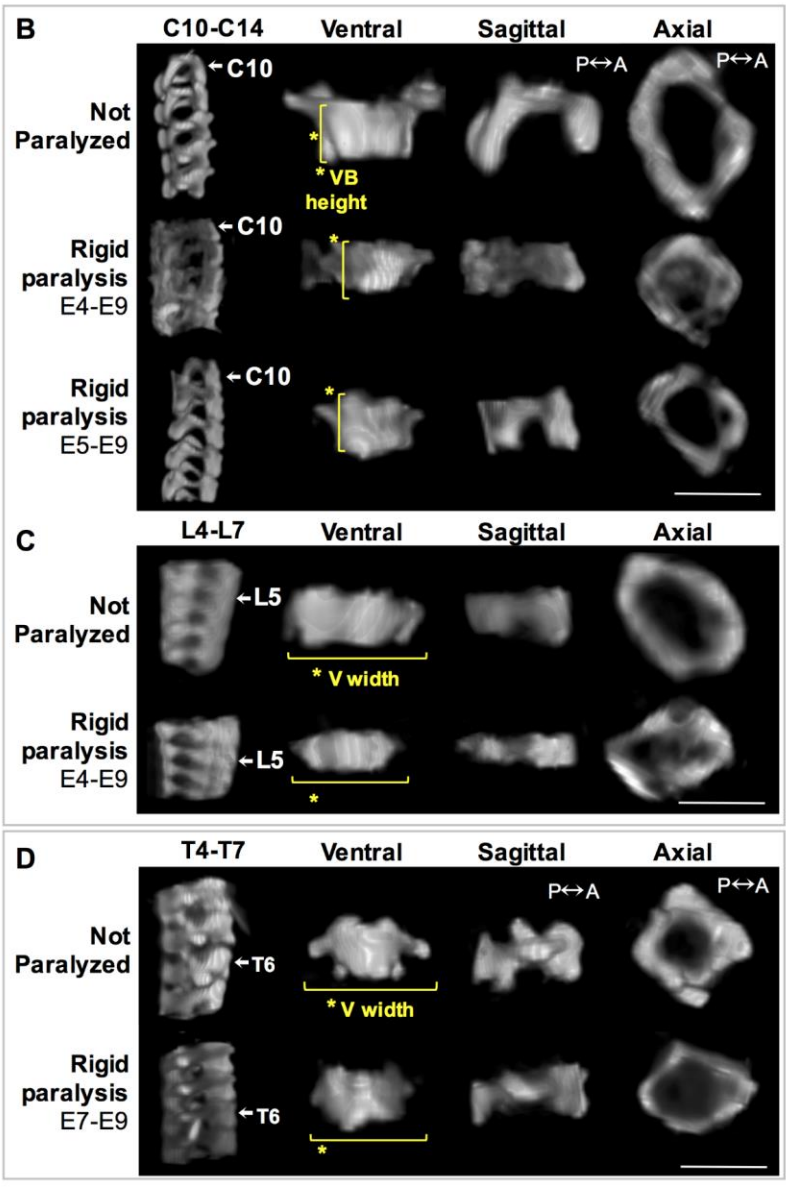
B
C10-C14
Ventral
Sagittal
Axial
P↔A
P↔A
Not Paralyzed
C10
* VB height
Rigid paralysis E4-E9
C10
Rigid paralysis E5-E9
C10
C
L4-L7
Ventral
Sagittal
Axial
Not Paralyzed
L5
* V width
Rigid paralysis E4-E9
L5
D
T4-T7
Ventral
Sagittal
Axial
P↔A
P↔A
Not Paralyzed
T6
* V width
Rigid paralysis E7-E9
T6

Figure 5: Initiation of rigid paralysis on or prior to E5 induced posterior vertebral cartilaginous fusion and discrete changes in vertebral shape, while paralysis on or after E6 showed normal segmentation but discrete shape changes in the thoracic region. (**A**) Sagittal alcian blue (cartilage) and picro–sirus red (collagen) stained sections of posterior spinous process (i, iii, v, vii, ix, xi, xiii) and anterior symphysis joints (ii, iv, vi, viii, x, xii, xiv) in control (i-ii) and timed rigid paralysis spines in the cervical region. Posterior vertebral fusion of the spinous process (sp) is indicated by the continuous cartilaginous staining (green arrows) as is fusion of the symphysis joints (SJ) (orange arrow). Scale bars100µm. P; posterior, A; anterior. (**B**) Representative sagittal 3D views of cervical spine segment (C10-C14) and ventral, sagittal and axial 3D views of C10 from control and rigid (E4–E9, E5-E9) paralysis groups. (**C**) Representative sagittal 3D views of lumbar spine segment (L4-L7) and ventral, sagittal and axial 3D views of L5 from control and rigid (E4-E9) paralysis groups. (**D**) Representative sagittal 3D views of thoracic spine segment (T4–T7) and ventral, sagittal and axial 3D views of T6 from control, rigid (E7–E9) paralysis. (**B-D**) Yellow lines indicate the significant differences with paralysis compared to controls. Scale bar 1000µm.

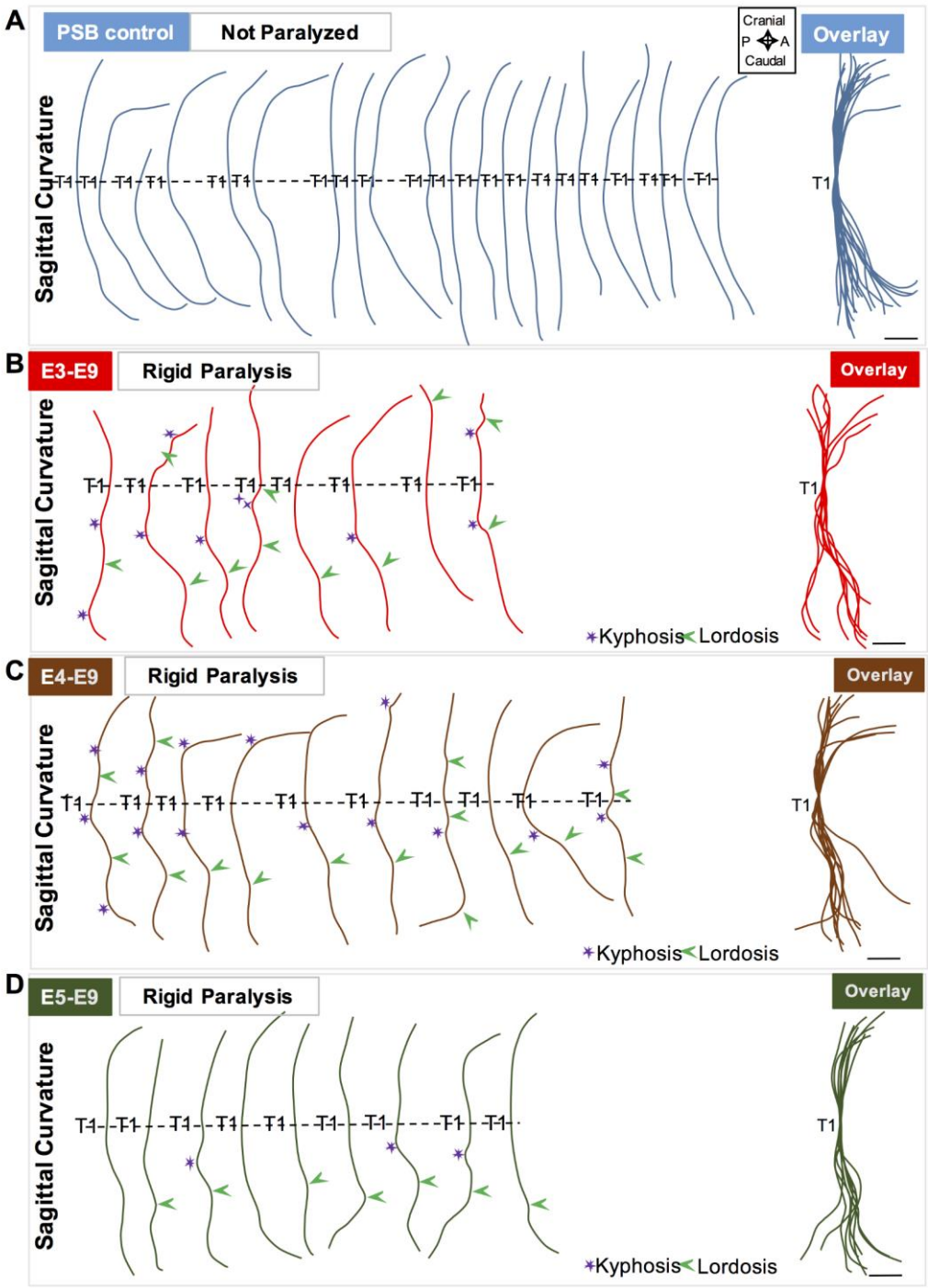

Supplementary Figure 1: Individual curvatures in the sagittal plane of (**B–D**) spines paralyzed on or prior to E5 compared to (**A**) control curvatures aligned to thoracic vertebra 1 (T1). Variation in control curvatures is evident, with more pronounced variation in the cervical and caudal regions depending on the position of the head, and the position of the embryonic pygostyle (plate of bone at the posterior end of the spine). Lordotic (green arrows) and kyphotic (purple stars) curvatures resulted from rigid paralysis, with more severe alterations observed in various sub-regions (**B**) from E3-E9, (**C**) E4-E9 and (**D**) E5-E9 paralyzed spines. Scale bars 2000µm

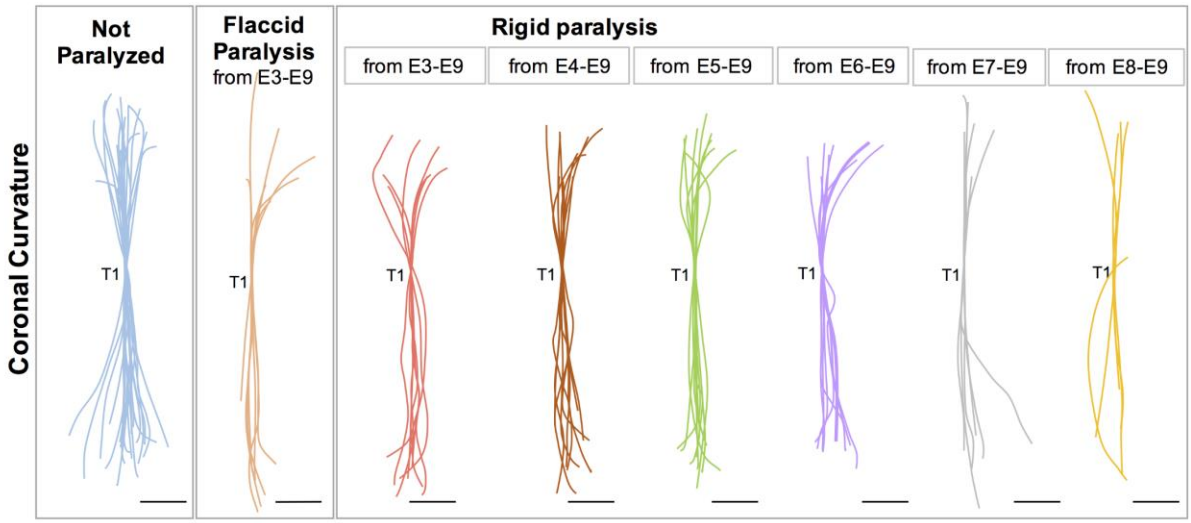

Supplementary Figure 2: Paralysis induced no pronounced changes in curvatures in the coronal plane. Overlays of curvatures in the coronal plane of control spines (n=21), prolonged flaccidly paralyzed spines (n=7), and rigidly paralyzed spines (E3–E9: n=8; E4–E9: n=10; E5–E9: n=9; E6–E9: n=8; E7–E9: n=6; E8–E9: n=5). All spines aligned to thoracic vertebra 1 (T1). Scale bars 2000µm.

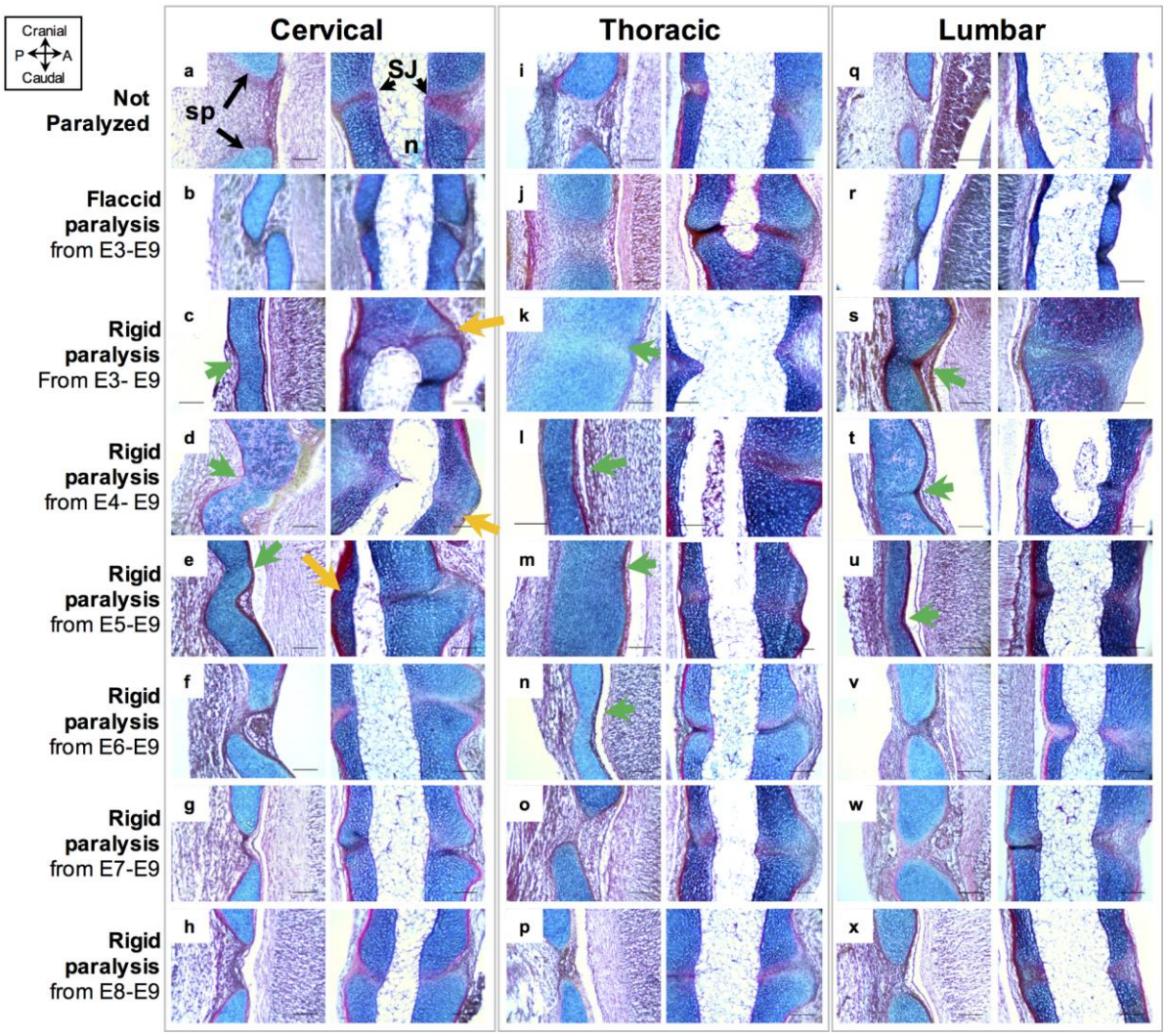

Supplementary Figure 3: Comprehensive histological analysis of vertebral segmentation in E9 spines following (b, j, r) flaccid paralysis and (c–h, k–p, s–x) rigid paralysis from multiple initiation time-points compared to controls (a, i, q). Sections stained with alcian Blue- cartilage/ picro-sirus red- collagen. sc: spinal cord, n; notochord. P; posterior, A; anterior. Scale bars 100µm.

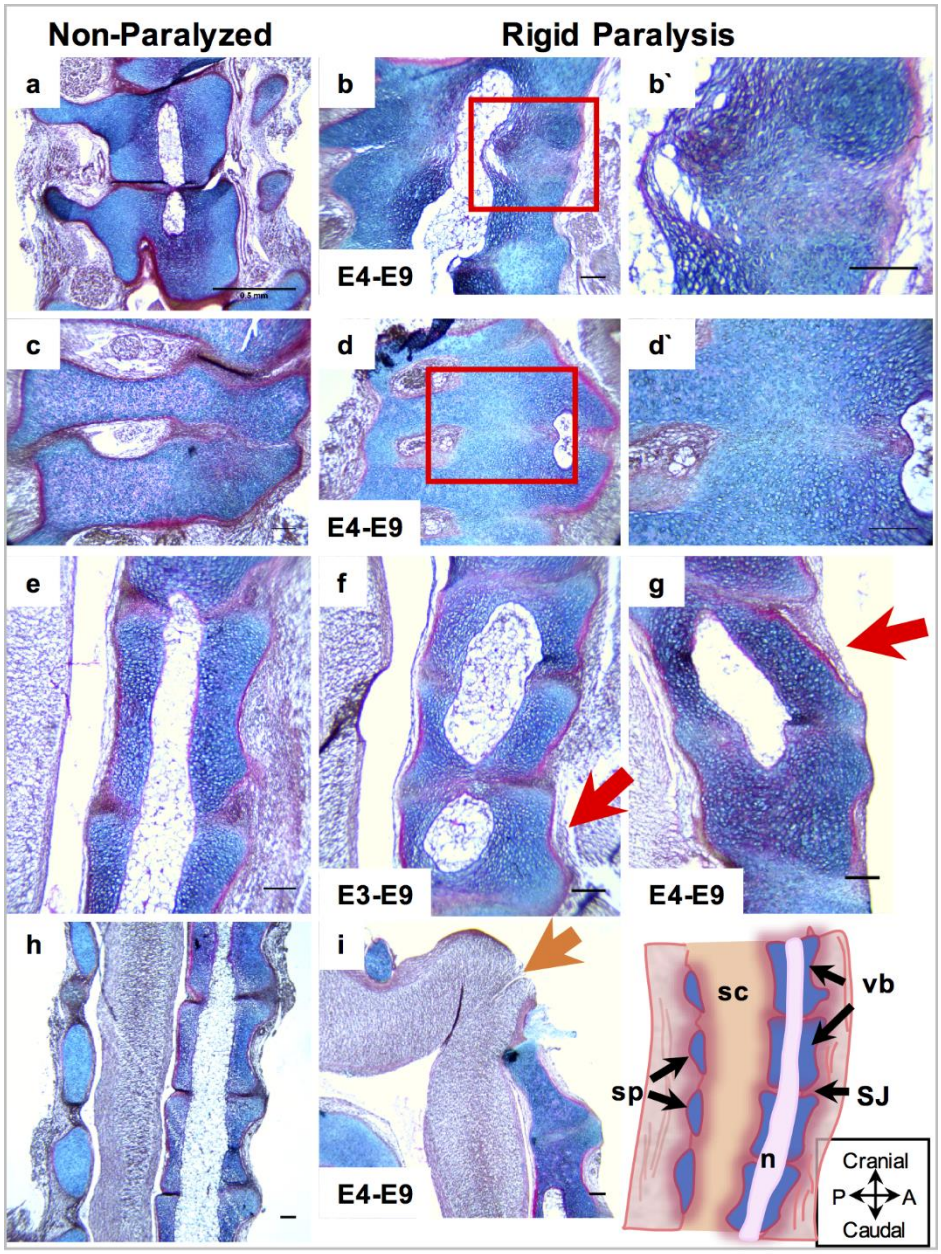

Supplementary Figure 4: Pathological changes in the vertebrae were observed following rigid paralysis commenced on or before E5. Dorsal (a–b) and lateral (c–d) views of paralyzed vertebrae show further evidence of vertebral fusion. (b' and d') are corresponding red boxes shown at higher magnifications. (f–g, red arrows) Distortions in normal sagittal cross-sectional shape of the vertebral bodies (vb) compared to (e) controls. A unique bending and anterior protrusion of the spinal cord (sc) was observed in one rigidly paralyzed specimen (i, orange arrow) compared to control (h) in which the spinal cord is enclosed within the vertebrae. Sp; spinous process, n; notochord, Scale bar in (a) 500µm, (b–i) 100µm.